

Geodetic measurements of postglacial adjustments in Greenland

Shfaqat Abbas Khan,¹ John Wahr,² Eric Leuliette,³ Tonie van Dam,⁴ Kristine M. Larson,⁵ and Olivier Francis⁴

Received 26 January 2007; revised 19 October 2007; accepted 27 November 2007; published 14 February 2008.

[1] We analyze data from seven continuous Global Positioning System (GPS) receivers and one tide gauge, all located along the edge of the Greenland ice sheet, to determine vertical uplift rates. We compare our results with predictions based on the ICE-5G deglaciation model of Peltier (2004). Results from the GPS receiver at Kellyville (-1.2 ± 1.1 mm/a) and from the tide gauge at Nuuk (-2.2 ± 1.3 mm/a), indicate that ICE-5G overestimates the subsidence rates at those locations by 2.1 and 1.1 mm/a, respectively. Kellyville and Nuuk are located along the southwestern margin of the Greenland ice sheet, and the observed negative uplift rates are consistent with independent evidence that the ice margin along the southwestern edge readvanced during the last ~ 8 ka to its current position. The ICE-5G glaciation-deglaciation history includes a readvance between the latitudes of 62°N and 72°N . The GPS measurements suggest the ICE-5G readvance may be too large or mistimed. Our GPS results at Qaqortoq, located at the southern tip of Greenland, suggest a secular subsidence rate of -0.3 ± 1.1 mm/a, while ICE-5G predicts an uplift rate of 1.0 mm/a. ICE-5G assumes no ice sheet readvance in south Greenland, including no readvance of the Qassimiut lobe. The difference of 1.3 ± 1.1 mm/a can tentatively be explained as due to a ~ 33 km readvance of the Qassimiut lobe during the last ~ 3 ka. For the other GPS sites, the observed/predicted uplift rates are $3.6 \pm 1.1/-0.1$ mm/a at Thule, $0.0 \pm 1.1/2.0$ mm/a at Scoresbysund, and $-0.4 \pm 1.1/-1.7$ mm/a at Kulusuk. For Thule, Kulusuk, and Scoresbysund the differences between the observed and predicted rates are on the order of 1.3–3.7 mm/a, though with opposite signs, and indicate that ICE-5G does not exactly reproduce the correct rebound signal at those locations.

Citation: Khan, S. A., J. Wahr, E. Leuliette, T. van Dam, K. M. Larson, and O. Francis (2008), Geodetic measurements of postglacial adjustments in Greenland, *J. Geophys. Res.*, 113, B02402, doi:10.1029/2007JB004956.

1. Introduction

[2] The Earth is still rebounding from the deglaciation that followed the Last Glacial Maximum (LGM), $\sim 20,000$ years ago. Observations of the rebound can provide information about the temporal and spatial patterns of that deglaciation, as well as about the Earth's viscosity profile. Greenland lost considerable ice during this deglaciation period. However, because it is still largely ice covered, there are relatively few rebound observations available to help constrain its ice history. As a result, Greenland deglaciation models are not nearly as well con-

strained as are the corresponding models for Canada or Scandinavia.

[3] A more uncertain ice model means that predictions of the rebound are also more uncertain. One consequence is that it is harder to confidently model and remove Greenland rebound effects from other kinds of observations, to study other processes. For example, present-day ice mass changes in Greenland are now being regularly monitored with laser and satellite altimetry, and with satellite gravity. These observations must be corrected for contributions from the rebound signal. Satellite gravity is particularly sensitive to that signal. Errors in the predicted rebound can thus lead to errors in the estimates of present-day mass imbalance.

[4] In this paper, we use Global Positioning System (GPS) and tide gauge observations to observe the ongoing glacial isostatic adjustment in Greenland. The results can be used to assess existing models and to constrain future models. This work is an extension of a previous study [Wahr *et al.*, 2001] that used data from continuously recording GPS receivers at Kellyville (KELY) and Kulusuk (KULU) (Figure 1) to conclude that the area near KELY is subsiding due to the Earth's viscoelastic response to past ice mass variability. They found that KELY and KULU are

¹Danish National Space Center, Technical University of Denmark, Copenhagen, Denmark.

²Department of Physics and Cooperative Institute for Research in Environmental Sciences, University of Colorado, Boulder, Colorado, USA.

³Colorado Center for Astrodynamics Research, University of Colorado, Boulder, Colorado, USA.

⁴Faculty of Sciences, Technology and Communication, University of Luxembourg, Luxembourg, Luxembourg.

⁵Department of Aerospace Engineering Sciences, University of Colorado, Boulder, Colorado, USA.



Figure 1. Locations of the GPS sites (red dots), the tide gauge station (red triangle), DYE3 (yellow triangle), and Paamiut (green triangle).

sinking by 5.8 ± 1.0 mm/a and 2.1 ± 1.5 mm/a, respectively. They explained the subsidence at KELY as the result of an advance of the nearby ice margin during the last 4000 years, although the area had been deglaciating prior to that. This interpretation is supported by geological evidence that shows the ice sheet in this region may have advanced by about 50 km during the last 4000 years [Huybrechts, 1992; van Tatenhove *et al.*, 1996]. That evidence, as well as the GPS results, were used by both Tarasov and Peltier [2002] and Fleming and Lambeck [2004] to constrain and assess their Greenland deglaciation models. Both Tarasov and Peltier [2002] and Fleming and Lambeck [2004] explained the subsidence at KELY as a combination of an advance of the nearby ice margin and collapse of the fore bulge that surrounded the former North American ice sheets. The GrB model of Tarasov and Peltier [2002], for example, includes an advance of the entire western margin between 62°N and

72°N during the last 8000 yrs, resulting in present-day crustal subsidence along the west coast.

[5] The geological studies that suggest a readvancing ice margin were conducted only near Kangerlussuaq (about 20 km from KELY). Also, Wahr *et al.*'s [2001] GPS results in west Greenland were only from the one location. The GPS coverage of this area was extended by Dietrich *et al.* [2005], who reported results for 1995–2002 from a network of 10 repeatable GPS sites, with observations carried out over a couple of weeks per year at intervals of 1–7 years. Dietrich *et al.* [2005] found that the area near the western ice margin between Paamiut (latitude 62.98°N , longitude 45.67°W) and Kangerlussuaq (latitude 67.00°N , longitude 50.68°W) is sinking by 2–4 mm/a; but that there is a significant east-west gradient to this subsidence rate, with smaller rates to the west.

[6] Here, we further expand the set of observational constraints, from both the southwest coast and elsewhere in Greenland, using data from a wider set of continuously recording instruments than Wahr *et al.* [2001] had access to, as well as reanalyzing longer data spans from KELY and KULU. Most of these data are from GPS receivers. However, there are also data from one tide gauge, at Nuuk in west Greenland (Figure 1). A tide gauge measures changes in sea level relative to the surface of the crust, and so its output contains contributions both from solid Earth displacements (e.g., tectonic processes, glacial isostatic adjustment following removal of ice) and from eustatic signals in the ocean (e.g., changes in water mass or density). The separation of the solid Earth and eustatic signals can be obtained by using satellite altimetry data. The difference between the tide gauge and the altimetry observations gives an estimate of vertical crustal motion.

2. Observations

2.1. GPS Data

[7] In May 1995, Kort og Matrikel-Styrelsen (KMS) established a permanent GPS station, Thule 1 (THU1), at Thule Air Base (see Figure 1). Data acquisition has been continuous, except for gaps in 1997 and 2001 due to failure in the connection between the receiver and antenna. The THU1 GPS antenna is mounted on the roof of an apartment building owned by the U.S. Air Force. In March 1999, KMS established a second GPS station, Thule 2 (THU2), at Thule Air Base, 963.31 m from THU1. The THU2 antenna is supported on a concrete pillar set in bedrock. The THU2 data contain relatively large gaps in 1999 and 2000, but since 2000 the station has been collecting data without significant interruption.

[8] KMS also operates a permanent GPS station at Scoresbysund 1 (SCOB). The GPS station was established in August 1997 and removed in October 2005. As a replacement for SCOB, the station Scoresbysund 2 (SCOR) was established in September 2004. Here we use data from both sites. From August 1997 to 11 September 2004 we use SCOB data and from 11 September 2004 to present we use SCOR data. The distance between SCOB and SCOR is 21.86 m. We denote the combined time series of SCOB and SCOR as SCBB.

[9] KMS also maintains a permanent GPS station at Qaqortoq (QAQ1), established in October 2001. The GPS

Table 1. Dates of Station Installations and Antenna Replacements

Site	Date Installed	Antenna Type	Receiver Type
Kellyville (KELY)	23 Jul 1995	AOAD/M T DOME	ROGUE SNR-8000
	5 Apr 1996	AOAD/M T DOME	ROGUE SNR-8000
	14 Sep 2001	ASH701945C M	ASHTECH Z-XII3
Thule 1 (THU1)	2 May 1995	AOAD/M T	ROGUE SNR-12 RM
Thule 2	6 Oct 1998	ASH701073.1 DOME	ASHTECH Z18
	17 Nov 2000	ASH701073.1 SCIS	ASHTECH Z18
	9 Aug 1997	TRM29659.00	TRIMBLE 4000SSI
Scoresbysund 1 (SCOB)	20 Oct 2005	Station removed!	Station removed!
Scoresbysund 2 (SCOR)	27 Oct 2004	ASH701941.B	ASHTECH UZ-12
Kulusuk (KULU)	21 Jul 1996	TRM22020.00+GP DOME	TRIMBLE 4000SSI
	9 May 1999	TRM29659.00 SCIT	TRIMBLE 4000SSI
Qaqortoq (QAQ1)	15 Oct 2001	ASH701941.B SCIS	ASHTECH UZ-12
	5 Sep 2003	ASH701941.B	ASHTECH UZ-12
	29 Sep 2003	ASH701941.B SCIS	ASHTECH UZ-12
	30 Dec 2003	ASH701945E M SCIS	ASHTECH UZ-12

antenna at QAQ1 was replaced three times during 2003. On 26 August 2003, the original antenna was damaged due to extreme weather conditions (the antenna was actually blown off the pillar). On 5 September the antenna was placed back on the pillar but without the damaged dome. A new dome was mounted on the antenna on 29 September 2003.

[10] The University of Colorado installed a GPS station at KELY in July 1995 and one at KULU in July 1996. There have been two antenna replacements at KELY and one at KULU. The dates of all antenna replacements, and the antenna and receiver types, are listed in Table 1. THU1, THU2, KELY, SCOR, and QAQ1 are all included in the IGS network.

2.2. Tide Gauge Data

[11] The tide gauge data used in this study were collected by Farvandsvnet (FRV) in Denmark. In 1992, FRV installed a tide gauge at Nuuk (also known as Godthaab) on the west coast of Greenland (see Figure 1). The instrument was placed at the bottom of a well to protect it from flowing objects. It consists of a pressure sensor to measure bottom pressure variations, and additional instruments to measure the temperature and salinity of the water. In summer 2004 the Nuuk tide gauge stopped operating in Nuuk and was moved to a new location at Thule Air Base, where it is now being administered by the Danish National Space Center. During twelve years of measurements at Nuuk, there were three large gaps caused by freezing of the water during winter. The instrument survived the other winters without data loss.

3. Analysis of the GPS Data

[12] To estimate site coordinates we use the GIPSY OASIS II software [Zumberge *et al.*, 1997] developed at the Jet Propulsion Laboratory (JPL). We use GPS orbits, earth orientation, and clock products provided by JPL, based on a global network of GPS sites. Receiver clock parameters and atmospheric parameters are modeled and a minimum elevation angle (also known as the cutoff angle) of 5° is used. The impact of the minimum elevation angle on secular uplift rates is described in section 3.3. The data are corrected for the solid earth tide and ocean tide loading.

The amplitudes and phase lags of the main ocean tide loading signal are calculated using the online program provided by H.-G. Scherneck (H.-G. Scherneck and M. S. Bos, <http://www.oso.chalmers.se/~loading/>). The GOT00.2 [Ray, 1999] ocean tide model is used for the loading correction. Site coordinates for each day are obtained using GIPSY OASIS II's Precise Point Positioning (PPP) strategy. The site coordinates are computed in the nonfiducial frame and transformed to the ITRF2005 frame [Altamimi *et al.*, 2007]. The transformation parameters (x files) from the free-network estimates to the ITRF2005 reference frame for a particular day are obtained from M. Heflin (personal communication, 2007).

[13] The International Terrestrial Reference Frame (ITRF) provides the definitive realization of the terrestrial origin, scale, orientation, and their time derivatives. The current reference frame used worldwide for geodetic applications is the ITRF2005 [Altamimi *et al.*, 2007]. The origin is defined as the center of mass (CM) of the whole Earth (including ocean and atmosphere) determined from Satellite Laser Ranging (SLR) solutions. The scale and scale rate is defined by nullifying the scale and its rate with respect to very long baseline interferometry (VLBI) time series. Although the ITRF2005 origin and its drift are determined with high accuracy, and the ITRF2005 is the most accurate frame ever developed, it still contains errors.

[14] Recently, Altamimi *et al.* [2007] found a 1.8 mm/a change in the z component of the origin between ITRF2000 [Altamimi *et al.*, 2002] and the ITRF2005, suggesting that the CM is constrained poorly by SLR. This drift has a significant impact on our secular uplift rates for sites in Greenland. Transforming velocities from ITRF2000 to ITRF2005 will increase the vertical velocities in Greenland by more than 1 mm/a. The z component of the ITRF2005 origin seems to be drifting. Hence our uplift rates obtained using PPP with ITRF2005, are not directly comparable with those predicted by the ICE-5G glaciation/deglaciation history. To compare our GPS uplift rates with those predicted by ICE-5G, we use the reference frame of Argus [2007]. The origin of the reference frame of Argus [2007] is defined as the center of mass of the solid Earth (CE). For simplicity we denote the reference frame of Argus [2007] as CE2007. CE2007 lies about 1/3 of the way from ITRF2000 to

ITRF2005 and transformation from ITRF2000 to CE2007 can be obtained by adding 0.1 mm/a to X, -0.1 mm/a to Y, and 0.6 mm/a to Z. The CE2007 reference frame is believed to be moving no faster than 0.5 mm/a relative to CM. The velocity of CE2007 estimated by *Argus* [2007] is believed to be nearest the true velocity of CM than is the velocity of CM estimated using SLR (see *Argus* [2007] for details). Here, we use CE2007 as default.

3.1. Regional Filtering of the GPS Data

[15] Since we are only interested in secular trends, we first filter the GPS data using a “regional filter” to remove spatially correlated variations. Earlier studies [e.g., *Wdowinski et al.*, 1997] used a stacking method based on computing a daily common mode to improve the signal-to-noise ratio, which is important for vertical displacements. *Johansson et al.* [2002] investigated the use of empirical orthogonal function (EOF) analysis for the same purpose. Here, we illustrate our method of determining the regional signal, and of how that signal is applied as a correction to the GPS data at KELY.

[16] Figure 2a shows daily values of vertical positions at KELY. Each dot represents a daily solution. First we simultaneously fit two offsets (one for each antenna change), a secular trend, and annually and semiannually varying terms, to the daily vertical solutions. Each daily solution is weighted with the σ formal errors generated by the GIPSY OASIS II software and assumes those errors are uncorrelated from one day to the next. The two offsets occur at 5 April 1996 and 17 November 2001 (Table 1). The solid red line in Figure 2a shows the sum of the best fitting offsets, and annually, semiannually, and secularly varying terms. The dashed vertical line shows time of antenna replacements. Figure 2b shows the daily residuals at KELY, obtained by removing the fitted signal from the daily values of vertical positions.

[17] Figure 2c shows the daily vertical solutions for THU1 and THU2. The two stations are located less than a kilometer apart. Hence the secular uplift rate is assumed to be the same at both locations. However, the annual and semiannual signals are not identical at both sites, mainly because the two stations experience different multipath signals. To estimate secular displacements at Thule, data from both stations are used: THU1 from 2 May 1995 to 19 April 2001 and THU2 from 20 April 2001 to the present. A station change on 19 April 2001, is selected because it gives the fewest gaps and fewest antenna offsets for the combined THU1/THU2 time series, which we denote as THUL. Figure 2c (dots) shows the daily vertical solutions for THUL. The dashed vertical line on 19 April 2001 marks the station change. Similar to the KELY fitting procedure, we fit an offset, and secular, annual, and semiannual terms to the daily THUL data. However, instead of simply fitting one annual and one semiannual term to the entire data, we fit one annual and one semiannual term to the THU1 data and another annual and semiannual term to the THU2 data. The 2 annual, 2 semiannual, 1 offset, and 1 secular terms are fitted simultaneously to the daily THUL data. Each daily solution is weighted with the σ formal errors generated by the GIPSY OASIS II software. The solid red curve in Figure 2c shows the best fitting displacements. Note the annual and semiannual terms are different before and after

the offset. Figure 2d shows the daily residuals at THUL. Similarly to THUL, we fit an offset, and two annual, two semiannual, and a secular term to the daily data at SCBB. The dots in Figure 2e show the daily values of vertical positions, and the solid red line shows the best fitting annual, semiannual and secular terms.

[18] The daily residuals shown in Figures 2b, 2d, and 2f are not entirely random. They arise from measurement errors, tropospheric modeling errors, satellite orbit errors, and loading from the atmosphere, ocean, and water/snow/ice on land. Some of these errors have similar effects at the different sites. By constructing a regional mean signal, we can reduce some of these common errors in our daily vertical solutions. To construct a regional mean signal we average the daily residuals at KELY, THUL and SCBB. We first remove the mean of each site’s residual time series. However, the time spans for those three stations are not exactly the same. Furthermore, there are data gaps at different times and of different lengths. If we simply remove the mean of each site’s residual time series and then construct the regional daily mean, we would introduce small offsets each time data from one site is missing. To overcome this problem we first find the days where data from all three sites are available. There are 2177 such days. We then correct each of the three residual time series for a mean value computed for only those days. We do not use data from QAQ1 and KULU when constructing the regional daily mean signal. QAQ1 has a relatively short time span, and KULU has several large data gaps and shows clear nonlinear excursions in the data. Figure 2g shows the regional daily mean signal.

[19] The effects of regional filtering are illustrated in Figure 2h. Figure 2h shows the same daily values but with the regional signal removed, and Figure 2i shows the daily residuals with the regional signal removed. There is a clear reduction of the scatter after removing the regional filter (compare Figure 2a with Figure 2h). Furthermore, the annual, semiannual, and secular variations become more obvious after regional filtering. The regionally filtered daily vertical displacements are used in our further analysis of the GPS data.

3.2. Secular Trends in the GPS Data

[20] Our method of determining secular trends in the GPS data is similar to that described by *Wahr et al.* [2001], except that here we first apply the regional filter as described above. We fit, to the filtered data, annually, semiannually, and secular varying terms, and offsets at the times of equipment changes. We construct daily residuals by removing the fitted signal from the filtered data. The residuals are a combination of measurement errors and mismodeled signal, and we use them as an estimate of the total error in the filtered daily data. To use those error estimates to compute an uncertainty for our secular trend solution, we must first determine how the errors are correlated in time. We do this by estimating the decorrelation time of the daily residuals.

[21] Figure 3 shows autocorrelation functions for KELY, THUL, SCBB, KULU and QAQ1 using regionally filtered daily residuals. The time lag, τ , is given in days, and the autocorrelation is normalized to 1 at $\tau = 0$. The two horizontal lines (dashed lines) denote the 95% confidence

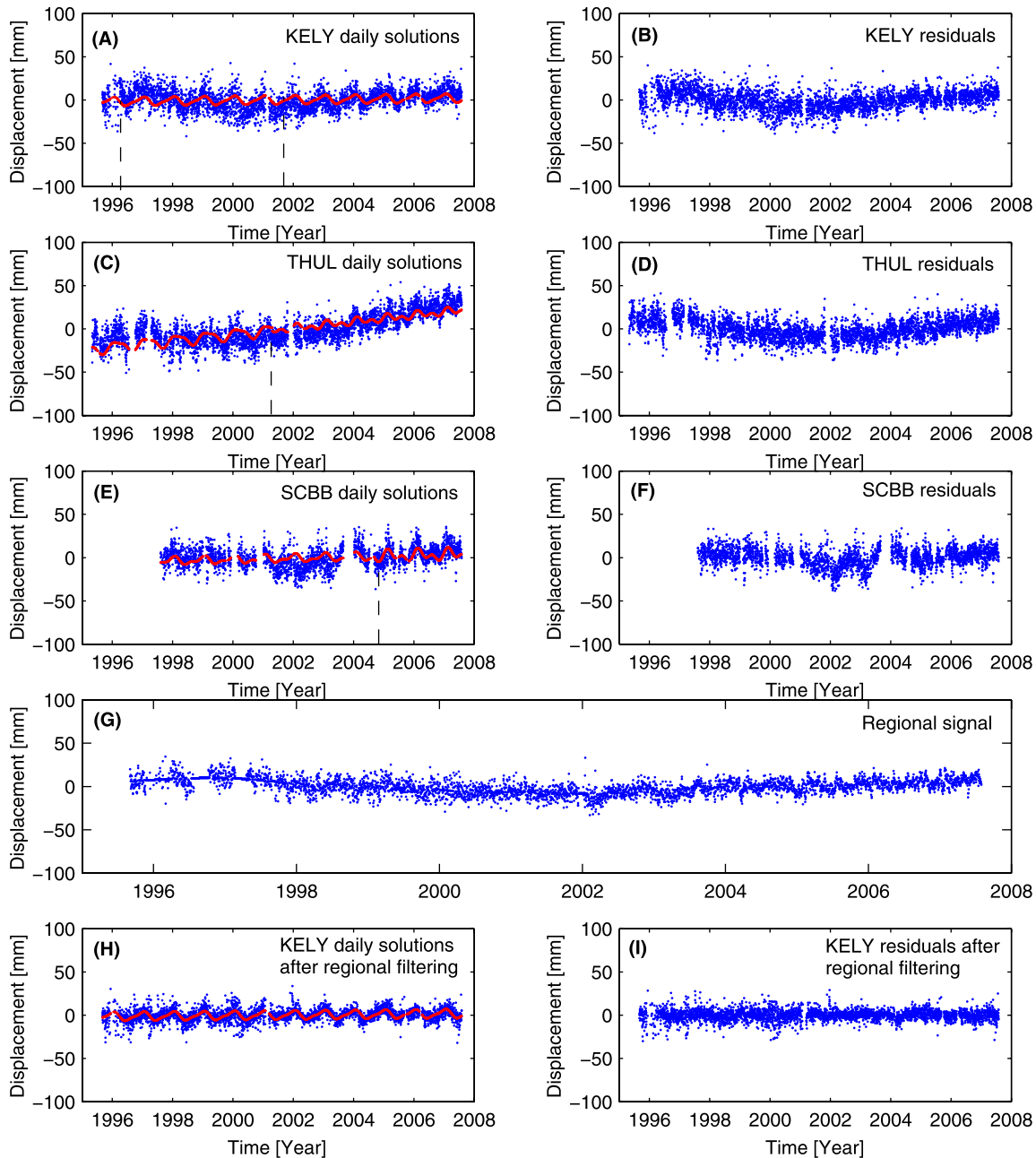


Figure 2. Daily values of vertical positions at (a) KELY, (c) THUL, and (e) SCBB (the solid curve shows the best fitting offsets, and the secular, annual, and semiannual terms), and daily residuals between the daily values and the solid curve at (b) KELY, (d) THUL, and (f) SCBB. (g) Regional daily mean signal. (h) Daily values of vertical positions at KELY after removing the regional signal shown in Figure 2g. (i) Daily residuals at KELY after removing the regional signal.

band. Figure 3 shows that the autocorrelation functions decrease significantly between $\tau = 0$ and $\tau = 1$. The autocorrelation function for KELY (Figure 3a) reaches the 95% confidence band when the time lag reaches 42 days. The autocorrelation function stays close to zero and inside the 95% confidence band for $\tau > 42$ d. Thus the function becomes statistically insignificant at lag times of about 42 d and longer. The autocorrelation function for THUL (Figure 3b) reaches its $\tau = \infty$ limit at a lag time of about 31 d. The autocorrelation function for SCBB decreases until

$\tau \approx 150$, then increases again until $\tau \approx 360$. This is an indication of a quasi-annual signal, which was not removed during the fitting process. During that process we fit an annual signal with constant amplitude. However, annual effects e.g., due to surface mass loads caused by the atmosphere, ocean, and water/snow/ice on land can have a varying amplitude. The autocorrelation function for SCBB reaches the 95% confidence band when the time lag reaches 88 d. The function does get outside the 95% confidence bands at longer lag times because of the quasi-annual signal.

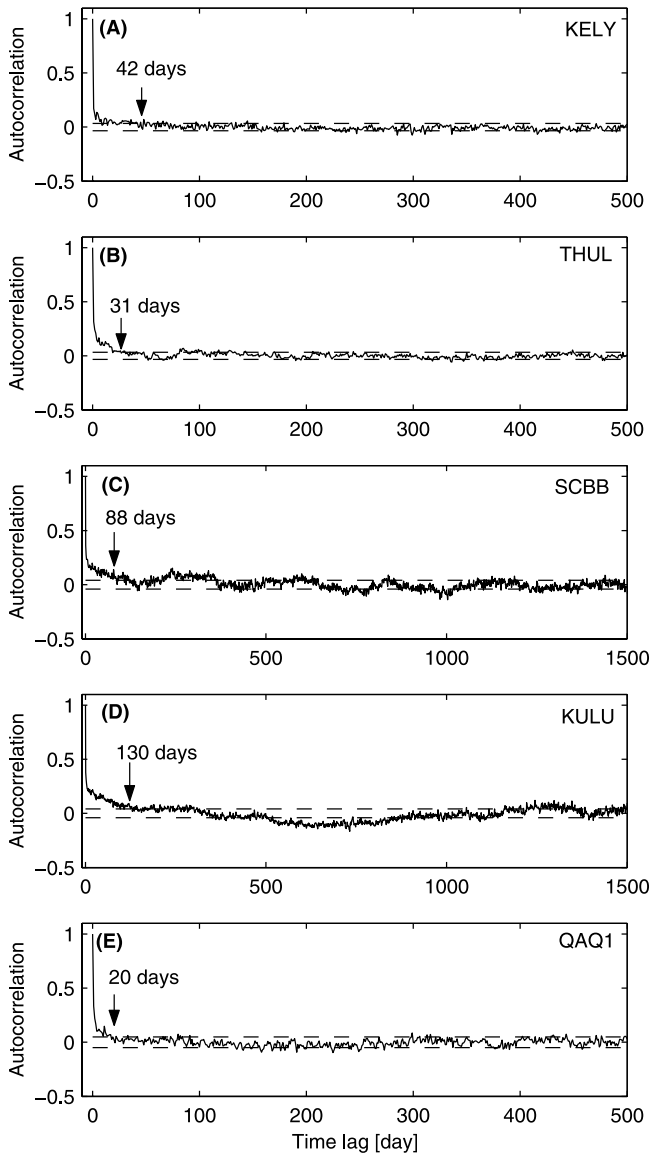


Figure 3. Autocorrelation functions at (a) KELY, (b) THUL, (c) SCBB, (d) KULU, and (e) QAQ1. The time lag is given in days and the autocorrelation is normalized to 1 at time lag = 0. The dashed horizontal lines denote the 95% confidence band.

However, the quasi-annual signal seems to be weak. Thus most of the time dependence in the data is taken into account when using a decorrelation time of 88 d. The autocorrelation function for KULU (Figure 3d) shows multiannual correlations. The function reaches the 95% confidence band when the time lag reaches 130 d. The function does get outside the 95% confidence bands at longer lag times because of the multiannual signal. Since the multiannual signal is weak we use decorrelation time of 130 d for KULU. The autocorrelation function for QAQ1 (Figure 3e) reaches and stays inside the 95% confidence band at lag times of about 18 d and longer. We use these decorrelation times to construct multiday averages of the daily residuals. For KELY, THUL, SCBB, KULU and QAQ1 we average over 42, 31, 88, 130, and 18 d, respectively.

[22] These averages are used to construct error estimates. Let σ_i denote the 1-sigma formal error of the i th day, as generated by the GIPSY OASIS II (PPP) software. This error estimate does not include orbit errors, tropospheric modeling errors, or multipath errors. A more realistic error can be obtained by multiplying the $1\sigma_i$ formal errors by a constant, c_m (the index m denotes the m th multiday interval, and c_m is only constant within this multiday interval). Consider the constant for the m th 42-d interval for KELY. Using χ^2 fitting [Press *et al.*, 1992], we fit an average value to the daily residuals within the m th interval, after assigning each daily residual an error of $\sigma_{c,i} = 1\sigma_i c_m$. The constant, c_m , is obtained by requiring that the final value of χ^2 equal the number of degrees of freedom (number of observations minus number of unknowns). The $\sigma_{c,m}$ are thus based on the scatter of the daily values about their mean within the m th interval. However, the mean value of the daily residuals is also an error and therefore add it (in quadrature) to $\sigma_{c,m}$, to obtain a final estimate of the uncertainty in the m th 42-d value. The errors we estimate provide a more realistic error estimate than the $1\sigma_i$ values, in that they include the effects of temporally correlated errors: e.g., orbit errors, tropospheric modeling errors, and multipath errors.

[23] Assigning our estimated errors to the 42-d averages at KELY, we simultaneously fit offsets, and annually, semiannually, and secular varying terms to the 42-d averages. Figure 4a shows the multiday averages at KELY and their assigned errors. The solid red line shows the best fitting offsets, and annual, semiannual, and secular terms. Figures 4b to 4e show similar plots for THUL, SCBB, KULU, and QAQ1.

[24] For KELY we obtain a secular uplift rate of 0.2 ± 0.1 mm/a (using the CE2007 reference frame). However, the uncertainty due to reference frame drift is not included in this error estimate. The frame uncertainty is 1.1 mm/a and can be included by adding it in quadrature to the error for the secular uplift rate obtained with the procedure described above. Our best secular uplift rate for KELY including all error considerations is 0.2 ± 1.1 mm/a. We use the differences in secular uplift rates obtained using CE2007 (Table 2) and ITRF2005 (Table 2), respectively, as an expression of the frame uncertainty.

[25] For THUL we obtain a secular uplift rate of 3.9 ± 0.2 mm/a when the reference frame uncertainty is not included and for SCBB we obtain a secular uplift rate of 0.9 ± 0.3 mm/a. Secular uplift rates including frame uncertainty at THUL, KELY, SCBB, KULU, and QAQ1 are listed in Table 2. Table 2 shows the observed secular uplift rates transformed to the ITRF2005.

[26] Figures 5a and 5b show convergence plots of uplift rates for KELY and illustrates the robustness of the secular varying term. The plots are obtained by fitting offsets, plus annual, semiannual, and secular terms to the first 500 d of observations. Then we add 42 days of data (since 42 d is the decorrelation time for KELY) and repeat the fit, add another 42 d and fit, etc.

[27] Each secular solution is plotted as a dot in Figure 5 and the vertical lines describe the estimated uncertainties of the secular uplift (the reference frame uncertainty is included in the error bars). The time represents the termination time of the data span used to estimate the secular uplift rate. The convergence plot in Figure 5b is obtained using the

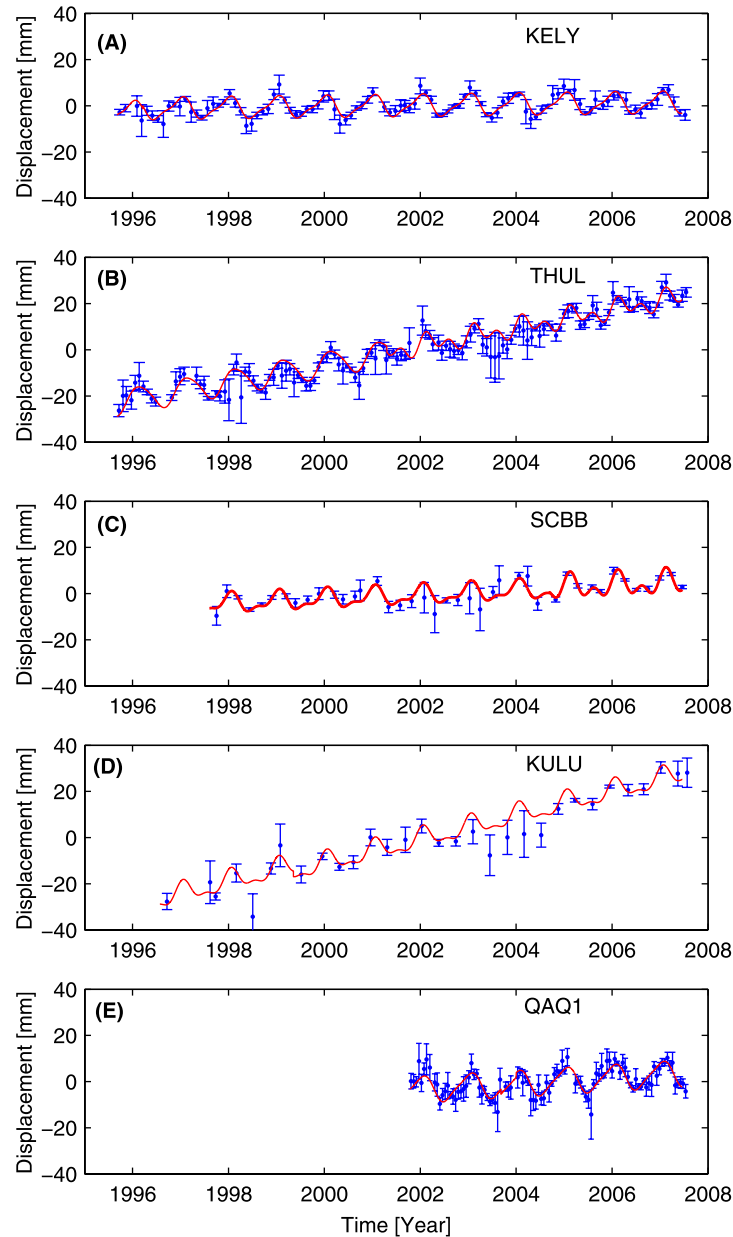


Figure 4. Multiday averages and their assigned errors at (a) KELY, (b) THUL, (c) SCBB, (d) KULU, and (e) QAQ1. The solid line shows the best fitting offsets, annual, semiannual, and secular terms.

regionally filtered data at KELY. The solutions have converged to 0.2 mm/a within our estimated $\pm 1.1 \text{ mm/a}$ uncertainty by the beginning of 2000, after only 4.5 years of data. Figure 5a shows a convergence plot for KELY using data that is NOT corrected for regional effects. These results do not converge to a constant rate. Figures 5a and 5b suggest that there are interannual signals at KELY and that they have a significant impact on the secular trend estimates when regional filtering is not applied. We infer that these signals are regionally correlated, since their effects are greatly reduced after regional filtering.

[28] Wahr *et al.* [2001] estimated a secular subsidence rate of $-5.8 \pm 1.0 \text{ mm/a}$ at KELY (the error includes the frame error). They used data collected between 1995.67 and 2001.15. They did not remove the regional signal in their

study. To compare our results with the results obtained by Wahr *et al.* [2001], we estimate an uplift rate at KELY using data that is not regionally filtered and that is collected between 1995.67 and 2001.15. We obtain a secular subsi-

Table 2. Observed Secular Uplift Rates and Their Uncertainties Using the CE2007 Reference Frame and the Observed Secular Uplift Rates Using ITRF2005^a

Site	CE2007, mm/a	ITRF2005, mm/a
KELY	0.2 ± 1.1	1.3
THUL	3.9 ± 1.1	5.0
SCBB	0.9 ± 1.1	2.0
KULU	5.2 ± 1.1	6.3
QAQ1	1.1 ± 1.1	2.1

^aBased on tide gauge and altimetry data.

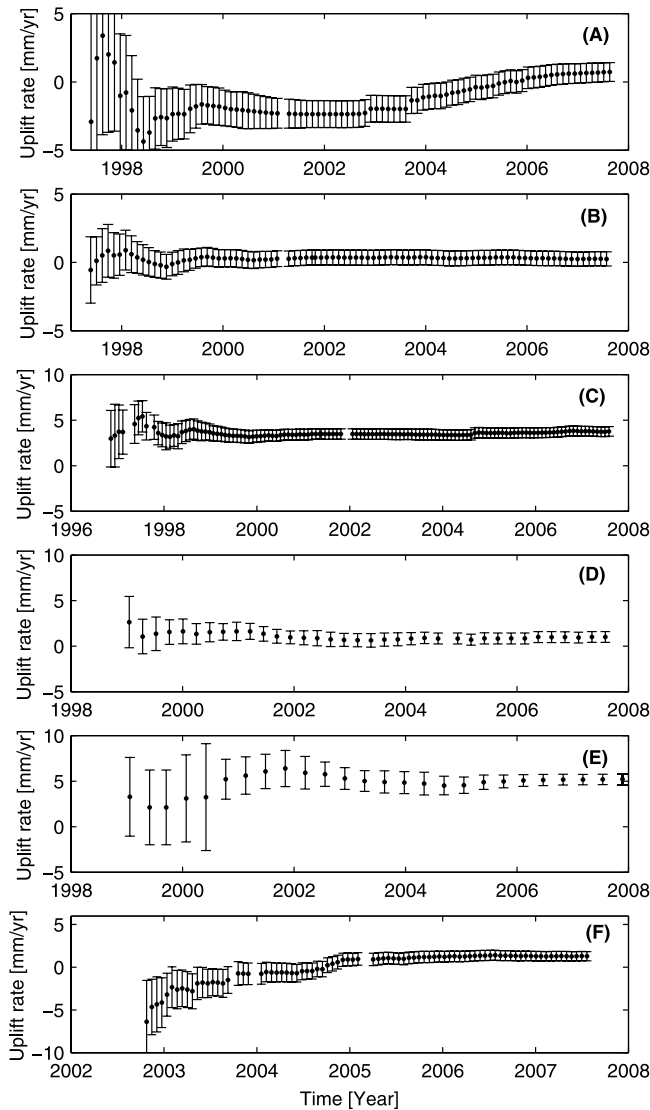


Figure 5. Convergence plots of uplift rates. (a) KELY (without regional filtering), (b) KELY (with regional filtering), (c) THUL (with regional filtering), (d) SCBB (with regional filtering), (e) KULU (with regional filtering), and (f) QAQ1 (with regional filtering).

dence rate of -2.3 ± 1.3 mm/a (see Figure 5a) at the termination time of 2001.15. The difference of about 3.5 mm/a between our results and the results of *Wahr et al.* [2001] is mainly due to the fact that here we use the CE2007 reference frame, while *Wahr et al.* [2001] used ITRF97. Moreover, we use cutoff angle of 5° , while *Wahr et al.* [2001] used 15° .

[29] Figures 5b to 5f show convergence plots of uplift rates at KELY, THUL, SCBB, KULU, and QAQ1 obtained using the regionally filtered data. The secular uplift solutions at KELY, THUL and SCBB appear to have converged to the final secular uplift rates given in Table 2, within 4.5–5 years. The GPS station at QAQ1 has been operating for almost 5 years. Thus we believe the secular uplift rate of 1.1 ± 1.1 mm/a at QAQ1 will not change much as the time span increases. The solutions at KULU seem to have converged to a constant secular uplift rate within the uncertainty.

However, KULU is affected by local, interannual effects caused by present-day ice mass changes [*Khan et al.*, 2007].

3.3. Minimum Elevation Angle and Secular Uplift Rates

[30] The GPS time series used in section 3.2 were obtained using the GIPSY OASIS II software with a minimum elevation angle of 5° . The default value for this angle is 15° when using the PPP strategy. However, an improved tropospheric correction can be obtained by using a lower minimum elevation angle. To study the influence this angle has on the secular uplift rate, we construct several time series at KELY using a different minimum elevation angle for each series. All other parameters, including the data time span, are held constant.

[31] Tropospheric effects are modeled within GIPSY OASIS II by estimating a stochastic zenith tropospheric delay and a stochastic tropospheric gradient at the GPS station. Additionally, the Niell function [Niell, 1996] is used as a mapping function. The zenith tropospheric delay and the tropospheric gradient are estimated as a random walk.

[32] We estimate site coordinates using minimum elevation angle of 15° , 10° , 5° and 2° . Figure 6 shows the respective autocorrelation functions for KELY obtained using the daily residuals for the various minimum elevation angles. Figure 6 shows that the autocorrelation decreases with decreasing minimum elevation angle, which is probably because the troposphere is better modeled when low elevation angles are used. On the other hand, the difference between using a minimum elevation angle of 2° , 5° or 10° is small.

[33] The 1σ formal errors generated by GIPSY OASIS II also decrease with decreasing minimum elevation angle. The reason could be that the tropospheric correction actually does improve when lower elevation angles are included, or it could be that the errors simply are underestimated. To further consider the effects of varying the minimum elevation angle, we compute 42-d averages and their $\sigma_{c,m}$ errors, as described above. We simultaneously fit offsets, and annual, semianual, and secular terms to those averages. Table 3 shows the secular uplift rates at KELY obtained using different minimum elevation angles. We have not applied any regional filtering, and the Table 3 uncertainties do not include reference frame errors. Table 3 shows that the uncertainty decreases with decreasing minimum elevation angle. Because a 5° elevation angle gives us the smallest uncertainty, we select a minimum elevation angle of 5° for our final uplift rates described in section 3.2.

[34] The Niell mapping function (NMF) is known to produce biases for high latitude stations and low elevation angles such as used in this study [Tregoning and Herring, 2006; Vey et al., 2006; Boehm et al., 2006]. Not using accurate surface pressure leads to errors in the station heights. Tregoning and Herring [2006] showed that this error can be large as 2 mm for annual variations. However, since we remove annual variations and our data time span is 5–12 years, the effect of not using actual surface pressure can be neglected.

4. Analysis of the Tide Gauge and Satellite Altimetry Data

[35] The satellite radar altimeter mission TOPEX/POSEIDON (T/P) provided sea level measurements with near-

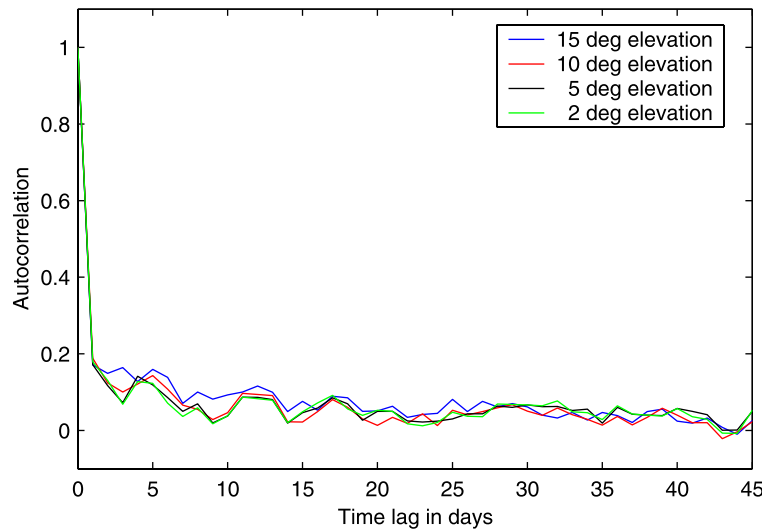


Figure 6. Autocorrelation functions at KELY for different minimum elevation angles.

global coverage (66°S – 66°N), 2–3 cm point-to-point accuracy, and 10-d temporal resolution from 1992 until 2005, greatly exceeding its design lifetime [Fu and Cazenave, 2000]. These measurements have continued with a successor mission, Jason-1, which was launched in 2001 into the original T/P orbit.

[36] T/P operated in several phases that in many respects can be treated as separate missions. In addition to the experimental POSEIDON altimeter, two distinct TOPEX altimeters operated. The primary TOPEX-A altimeter operated from shortly after launch until January 1999. After instrument degradation was observed starting in mid-1997, redundant backup TOPEX-B began to be used as the primary science instrument for the remainder of the mission. At the end of the verification phase of Jason-1, the original T/P mission ended in August 2002, and T/P was moved to a new orbit.

[37] To estimate a secular uplift rate at Nuuk from the tide gauge measurements there, sea surface height measurements are required. The time span of sea surface height time series has to be identical to the time span of the tide gauge time series. A time series of sea surface height measurements near the Nuuk tide gauge is constructed by computing a weighted mean of T/P and Jason-1 values sampled within 75 km of the station. Figure 7 shows 29 T/P along-track locations within 75 km of the station. The along-track sampling frequency of both missions is roughly 1 Hz, equivalent to 7 km. We use T/P data until 1 January 2002 and Jason-1 data after 1 January 2002.

[38] TOPEX data from Merged Geophysical Data Records Revision B (MGDRs) is used for cycles 10 to 364. Several modifications to the MGDRs have proved necessary. First, we replace the MGDR ocean and load tides with those from the GOT99.2 model, and equilibrium long-period ocean tides with those used for Jason-1. Second, the wet troposphere path delay is replaced with GDR Correction Product Version C, which corrects a drift in one channel on TOPEX and includes a TMR yaw correction to account for a slightly greater path delay when the satellite is in fixed rather than sinusoidal yaw [Zlotnicki and Callahan,

2002]. Finally, the MGDR sea state bias is replaced with the separate models estimated by Chambers *et al.* [2003] for TOPEX-A and TOPEX-B. These models remove most of the 3–7 mm bias between TOPEX-A and TOPEX-B that had been observed in the tide gauge calibrations of the original MGDR data.

[39] Jason data from a combination of GDR version A is used for cycles 22 to 127 and GDR version B for cycles 1 to 21 and 128 to 158. The wet troposphere path delay is replaced for version A cycles, to match the model used on version B. A 19 mm bias is removed from version A data to reconcile a bias between sea state bias models. A Jason-T/P bias is estimated using values observed during the 21 cycles of the verification phase, when T/P and Jason orbited in a tandem configuration and measurements were separated by 72 s.

[40] Because it is difficult to test the instruments once they are on-orbit, the calibration of the altimeter sea level measurements using tide gauge measurements has always been a critical component of sea level determination [Chambers *et al.*, 1998; Mitchum, 1994, 1998, 2000]. The drift during the original T/P mission estimated from the calibration is -0.1 ± 0.4 mm/a [Leuliette *et al.*, 2004]. The calibration error for T/P is almost entirely driven by errors in the land motion estimates used for each of the tide gauges [Mitchum, 2000]. The drift for Jason is -0.6 ± 0.8 mm/a.

[41] Finally, we remove variations in the sea surface attributable to a hydrostatic response to changes in atmospheric pressure, known as the instantaneous inverse barometer (IB) effect. The IB field available on the T/P

Table 3. Secular Uplift Rates at KELY Obtained Using Different Minimum Elevation Angles^a

Minimum Elevation Angle, deg	Uplift Rate (Using CE2007), mm/a
15	-0.14 ± 0.53
10	0.57 ± 0.49
5	0.72 ± 0.47
2	0.70 ± 0.48

^aThe rates are given in the CE2007 reference frame and obtained without applying a regional filter.

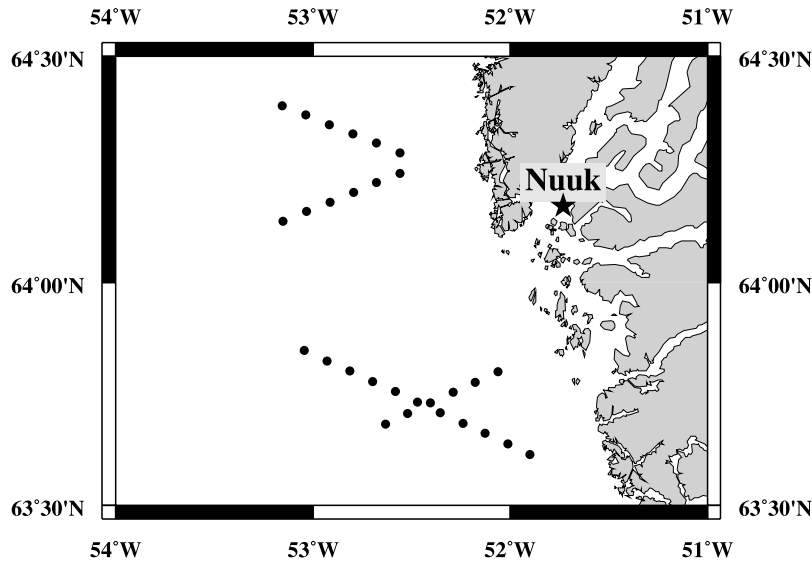


Figure 7. TOPEX/POSEIDON along-track points (black dots) near the tide gauge at Nuuk (black star).

MGRDs assumes a constant mean global surface pressure. We substitute the constant mean with time-varying mean pressure over the oceans computed from European Centre for Medium-Range Weather Forecasts (ECMWF) atmospheric pressure products to match the time-varying IB model on the Jason GDRs.

[42] The tide gauge data at Nuuk obtained from FRV has a sampling rate of 15 min. The data consist of relative sea level variations and atmospheric pressure observations. The inverse barometer effect is removed using

$$h_{IB} = -9.948(P_{obs} - P_g) \quad (1)$$

P_{obs} is the observed pressure in millibars at the tide gauge site and P_g is the mean pressure over the oceans in millibars.

The resulting inverted barometer correction, h_{IB} , is given in millimeters. The mean pressure over the oceans is interpolated from values determined at 6-h intervals from ECMWF. The ocean tides, h_{ot} , are removed from the observed relative sea level variation empirically (we fit and remove terms at the tidal frequencies). Thus

$$h_{residual} = h_{observed} - h_{IB} - h_{ot} \quad (2)$$

[43] Figure 8 shows monthly averages of the “interpolated altimetry measurements” minus the “tide gauge observations.” The solid line is the best fitting linear term. To estimate a secular uplift rate at Nuuk, an offset and a secular varying term are fitted simultaneously to the monthly averages. The offset is introduced at 1 January 2002,

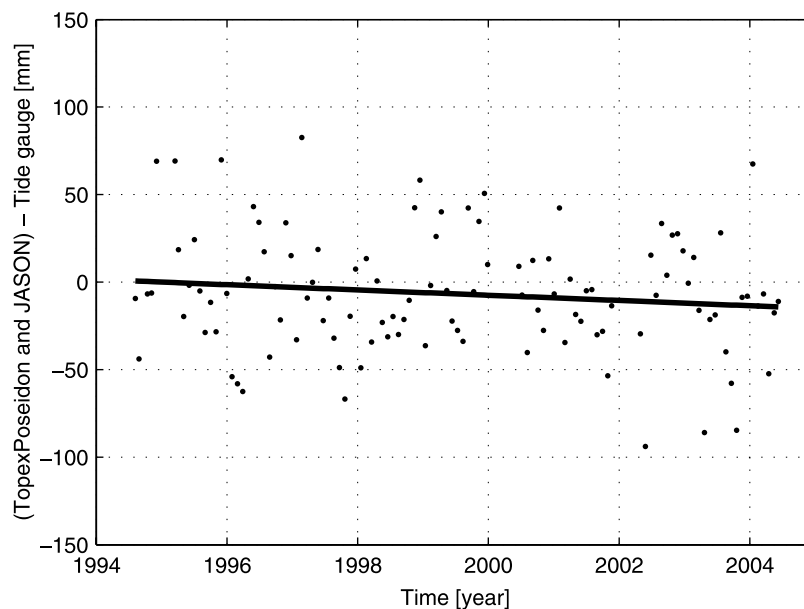


Figure 8. T/P and Jason measurements minus tide gauge observations. The solid line shows our best fitting trend.

Table 4. Predicted Uplift Rates at KELY, KULU, SCBB, THUL, and QAQ1 Due to Present-Day Ice Mass Changes of JG, HG, KG, and SG

Site	JG, mm/a	HG, + KG, mm/a	SG, mm/a	Regional Correction, mm/a	Total Uplift Rate, mm/a
KELY	0.5	0.4	0.6	0.0	1.4
THUL	0.1	0.2	0.1	0.0	0.3
SCBB	0.1	0.7	0.2	0.1	0.9
KULU	0.1	2.5	3.0	0.0	5.6
QAQ1	0.1	0.5	1.0	0.2	1.4
NUUK ^a	0.1	0.1	0.5	-	0.7

^aTide gauge site.

corresponding to the time when we change from T/P to Jason. Fitting the monthly mean variations using χ^2 fitting, we obtain a secular subsidence rate of -1.5 ± 1.3 mm/a at Nuuk.

5. Influence of Present-Day Ice Mass Changes

[44] All the GPS sites considered in this study are located near the edge of the Greenland ice sheet. Hence a portion of the observed secular uplift rates given in Table 2 could be due to the Earth's elastic response to ongoing changes in nearby ice.

[45] The Greenland ice sheet is mainly drained through its major outlet glaciers. Since 2000, the rates of ice discharge from Kangerdlugssuaq (KG) and Helheim glaciers (HG) in East Greenland and Jakobshavn glacier (JG) in West Greenland have more than doubled as a result of significant accelerations in flow speed [Rignot and Kanagaratnam, 2006; Dietrich *et al.*, 2007]. The sudden speed-ups of those glaciers coincided with observed thinning rates of 15–90 m/a [Joughin *et al.*, 2004; Stearns and Hamilton, 2007; Howat *et al.*, 2005] and indicate a significant mass imbalance in parts of the ice sheet.

[46] Rignot and Kanagaratnam [2006] used satellite radar interferometry observation to estimate mass loss of the Greenland Ice Sheet. To estimate the amplitude of the elastic motion due to thinning of JG, we assume the JG catchment gained ice at a rate of $4.6 \text{ km}^3/\text{a}$ during 1995–1996, and lost ice at a rate of $12.5 \text{ km}^3/\text{a}$ during 1997–2000 and $16.0 \text{ km}^3/\text{a}$ during 2001–2007. The rates are chosen to coincide with Rignot and Kanagaratnam's [2006] estimates of 1996, 2000, and 2005 ice volume changes in their area 20. For simplicity, we assume that all ice loss occurred near the JG grounding line.

[47] The largest 21 glaciers in southeast Greenland have accelerated in flow speed between 1996 and 2005 [Rignot and Kanagaratnam, 2006]. To model the crustal uplift caused by mass loss of the Southeast Glaciers (SG) (see Figure 1), we assume that ice sheet thinning occurred between 62°N and 66°N , and between sea level and 2500 m elevation [Krabbill *et al.*, 2004]. This region roughly corresponds to area 13 of Rignot and Kanagaratnam [2006]. Additionally, to coincide with Rignot and Kanagaratnam [2006], we assume SG lost ice at a rate of $29.3 \text{ km}^3/\text{a}$ during 1995–1996, $48.3 \text{ km}^3/\text{a}$ during 1997–2000 and $67.4 \text{ km}^3/\text{a}$ during 2001–2007.

[48] To estimate the amplitude of the elastic motion due to thinning of Kangerdlugssuaq and Helheim glaciers we use the rates of Khan *et al.* [2007] and Stearns and Hamilton [2007]. The rates of ice volume loss of HG and

KG are quantified using sequential digital elevation models using stereo satellite imagery collected by the ASTER (Advanced Spaceborne Thermal Emission and Reflection Radiometer) sensor. Khan *et al.* [2007] detected a total volume loss on KG of 310 km^3 during 2001–2006 (or $62 \text{ km}^3/\text{a}$) and a total volume loss on HG of 180 km^3 during 2002–2005 (or $60 \text{ km}^3/\text{a}$). Since HG and KG started to accelerate in 2000–2001, we assume no mass loss prior to 2001 on KG and prior to 2002 on HG. This is consistent with Table 1 of Rignot and Kanagaratnam [2006] which show no considerable mass changes on HG or KG in 1996 and 2000. We assume the KG catchment lost ice at a rate of $62 \text{ km}^3/\text{a}$ during 2001–2007, while we assume no mass loss prior to 2001. Furthermore, we assume the HG catchment lost ice at a rate of $60 \text{ km}^3/\text{a}$ during 2002–2007 and no ice loss occurred prior to 2002 nor between 2005 and 2006 [see Khan *et al.*, 2007]. We accurately account for the observed distribution of mass loss in the coastal regions using a 150×150 m grid [see Khan *et al.*, 2007, Figures 2c and 2d], while the catchment-wide volume losses are gridded to a coarser resolution of 5×5 km.

[49] Using the mass losses for JG, HG, KG and SG and convolving with Farrell's [1972] elastic Green's function for vertical displacements, we predict a corresponding total uplift rate at KULU of 5.6 mm/a . Hence most of the observed uplift at KULU is due to the Earth's elastic response to ongoing changes in ice. Table 4 shows the predicted uplift rates at KELY, KULU, THUL, SCBB, QAQ1 and NUUK due to present-day ice mass changes of JG, HG, KG and SG.

[50] Since the secular trends in the GPS data are obtained after removing the regional signal, we must also remove the regional contribution from the predicted elastic uplift rates. Table 4 shows the effect of the regional correction obtained in the same manner as described in section 3.1. Except that here we use predicted elastic uplift instead of GPS observed uplift. Table 4 also shows the total elastic uplift due to present-day mass ice mass changes of JG, HG, KG, and SG and after removing the regional contribution.

6. Comparison With Predictions From the ICE-5G Deglaciation Model

[51] The secular trends detected in the GPS measurements are presumably caused by a combination of the Earth's elastic response to present-day ice mass changes, and its viscoelastic response to ice mass changes in the past. In section 5 we estimated the effects of present-day changes. The GPS column in Table 5 shows the observed secular

Table 5. Observed and Predicted Secular Uplift Rates^a

Site	GPS, mm/a	ICE-5G(VM2), mm/a
KELY	−1.2	−3.3
THUL	3.6	−0.1
SCBB	0.0	2.0
KULU	−0.4	−1.7
QAQ1	−0.2	1.0
NUUK	-2.2 ± 1.3^b	−3.3

^aThe predicted rates are obtained by convolving viscoelastic Green's functions with the ice history of ICE-5G.

^bBased on tide gauge and altimetry data.

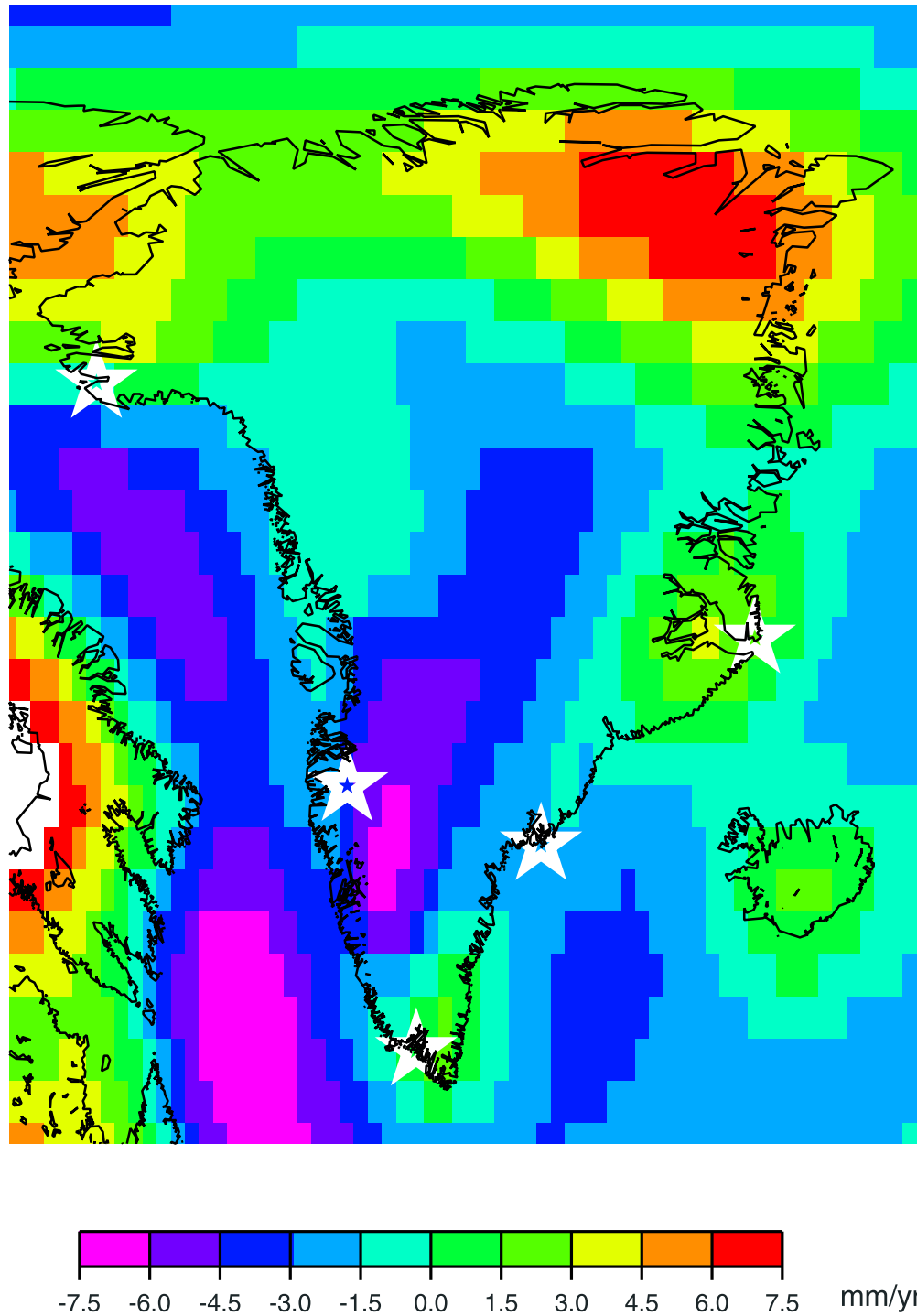


Figure 9. Map of predicted uplift rates (in mm/a) obtained by convolving viscoelastic Green's functions with the ice history of ICE-5G(VM2). Locations of GPS sites are marked with white stars.

uplift rates after removing the elastic effects of present-day ice mass changes.

[52] In this section, we consider the effects of past ice variability, both from Greenland and from the Canadian and Fennoscandian ice sheets. We use results based on deglaciation model ICE-5G of *Peltier* [2004], which is a global model and includes ice sheet histories for Greenland, Eurasia, North America, Antarctica and the British Isles.

For the Greenland component, ICE-5G uses the Greenland model of *Tarasov and Peltier* [2002].

[53] Reconstructions of deglaciation histories for a region are performed using geophysical inversion of observed relative sea level (RSL) histories [*Peltier*, 1994] or using glaciological models that incorporate descriptions of ice sheet dynamics [*Huybrechts*, 1996]. The GrB deglaciation model of the Greenland ice sheet [*Tarasov and Peltier*, 2002], uses a combination of both methodologies. GrB is

Table 6. Models of an Advancing Qassimiut Lobe^a

Model	Readvance d, km	Present-Day Uplift	Present-Day Uplift
		Without ICE-5G mm/a	With ICE-5G, mm/a
A	10	−0.3	0.7
B	20	−0.5	0.5
C	30	−0.7	0.3
D	40	−0.9	0.1
E	50	−1.1	−0.1
F	60	−1.3	−0.3
G	80	−1.7	−0.7
H	100	−2.0	−1.0
I	120	−2.2	−1.3

^aAll models assume the readvance started 3 ka ago and ended 150 years ago. The ice thickness at the margin is 200 m in each model and increases linearly to 1400 m at a distance of 120 km behind the margin. Present-day uplift rates at QAQ1 caused by a readvanced Qassimiut lobe and present-day uplift rates at QAQ1 including the ICE-5G prediction and the Qassimiut lobe readvance are shown.

incorporated into the global ICE-5G deglaciation model. The main difference between GrB and the Greenland components of earlier global models is that in GrB the mass of the Greenland ice sheet undergoes periods of increase subsequent to the mid-Holocene climatic optimum. In particular, the ice sheet margin in west Greenland (between latitudes of 62°N and 72°N) readvances to its present position during the last 8000 years, resulting in present-day subsidence of land along the west coast. In GrB, the readvance of the margin is about 40–60 km near Kangerlussuaq, decreasing to a few km or less at latitudes of 62°N and of 72°N. Figure 9 shows a map of predicted uplift rates obtained by convolving viscoelastic Green's functions based on viscosity model VM2 [Peltier, 2004], with the ice history of ICE-5G (uplift rates computed by D. Peltier and available from the International Earth Rotation Service, at http://www.sbl.statkart.no/projects/pgs/displacements/peltier_3d_disp_VM2.grid). All ice sheets are included in the ICE-5G estimates.

[54] Table 5 compares ICE-5G predicted uplift rates with the GPS results. The model shows differences on the order of 1.3–3.7 mm/a. At QAQ1, for example, the model predicts uplift whereas the GPS data indicate subsidence. Unlike its solution further north, the ICE-5G model suggests minimal or no ice sheet margin readvance near QAQ1 during the last 8000 years. The model suggests subsidence rate of −3.3 and −3.3 mm/a at KELY and Nuuk, respectively. Our GPS observations suggest subsidence rate of -1.2 ± 1.1 mm/a at KELY and our tide gauge observations suggest subsidence rate of -2.2 ± 1.3 mm/a at Nuuk. ICE-5G appears to be predicting too much readvance of ice along the west coast.

[55] The ICE-5G predicted present-day uplift pattern in North America is dominated by the presence of three distinct domes. One is over Ellesmere Island, where the maximum present-day uplift rate is about 8 mm/a. The deviation between observed and predicted uplift of about 3.7 mm/a at THUL can be explained by expanding the dome further to the east or by increasing the maximum ice thickness of the dome during LGM. Additionally, melting of ice caps and glaciers in north Greenland may also contribute significantly to the current uplift at THUL. The ice sheet in north Greenland experienced an extensive thinning in

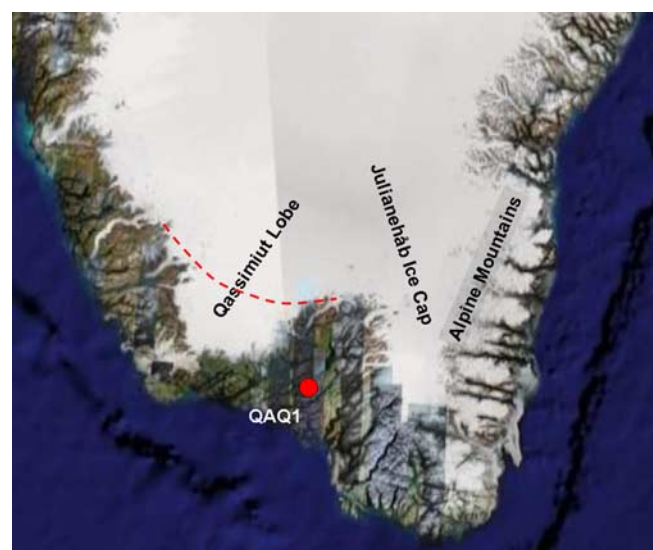
response to climate amelioration during the early Holocene [Landvik *et al.*, 2001].

7. Ice Sheet Evolution in Southern Greenland

[56] Here we discuss the ice sheet evolution in southern Greenland (south of 62°N), and especially those segments of the ice sheet, such as the Qassimiut lobe (see Figure 10), that experienced notably large changes in extent during the Holocene [Weidick *et al.*, 2004]. The inland ice margin in south Greenland lies mostly at elevations above 900 m, descending to lower levels at narrow outlet glaciers. In contrast, the Qassimiut lobe, about 100 km in width, is situated in a relatively low area, with its margin at an elevation below 500 m. East of the Qassimiut lobe is an area of high elevations, that contains the Julianehab Ice Cap situated along the Alpine Mountains.

[57] During the last glacial period most of the present deglaciated land area in this region was covered by ice. This is inferred from fresh erosional features on islands and coastal hills [Weidick *et al.*, 2004]. Basal lake sediment dating shows the ice cover may have extended even onto the continental shelf, with deglaciation beginning as early as 13.7 ka ago near the southern tip of Greenland. Abundant evidence in the form of basal lake sediment dates from sites close to the present ice margin shows that continued deglaciation reduced the ice sheet to its present dimensions at about 9.5 ka ago.

[58] The temperature several thousand years ago in this region, was warmer than it is today. Pollen records show the first indication of climate deterioration at about 3.4 ka ago in the area northwest to the Qassimiut lobe. A more marked change due to colder humid conditions began 3 ka ago in the vicinity of the Qassimiut lobe. Near the southern tip of Greenland and at coastal areas close to the Qassimiut lobe, cooling began about 2.1 ka ago [Fredskild, 1973; Weidick *et al.*, 2004]. This is consistent with reconstructed temperature history at DYE3 of the Greenland ice sheet [Dahl-Jensen *et al.*, 1998]. The temperature history reconstructed from present-day temperature measurements in bore holes after

**Figure 10.** Map of south Greenland.

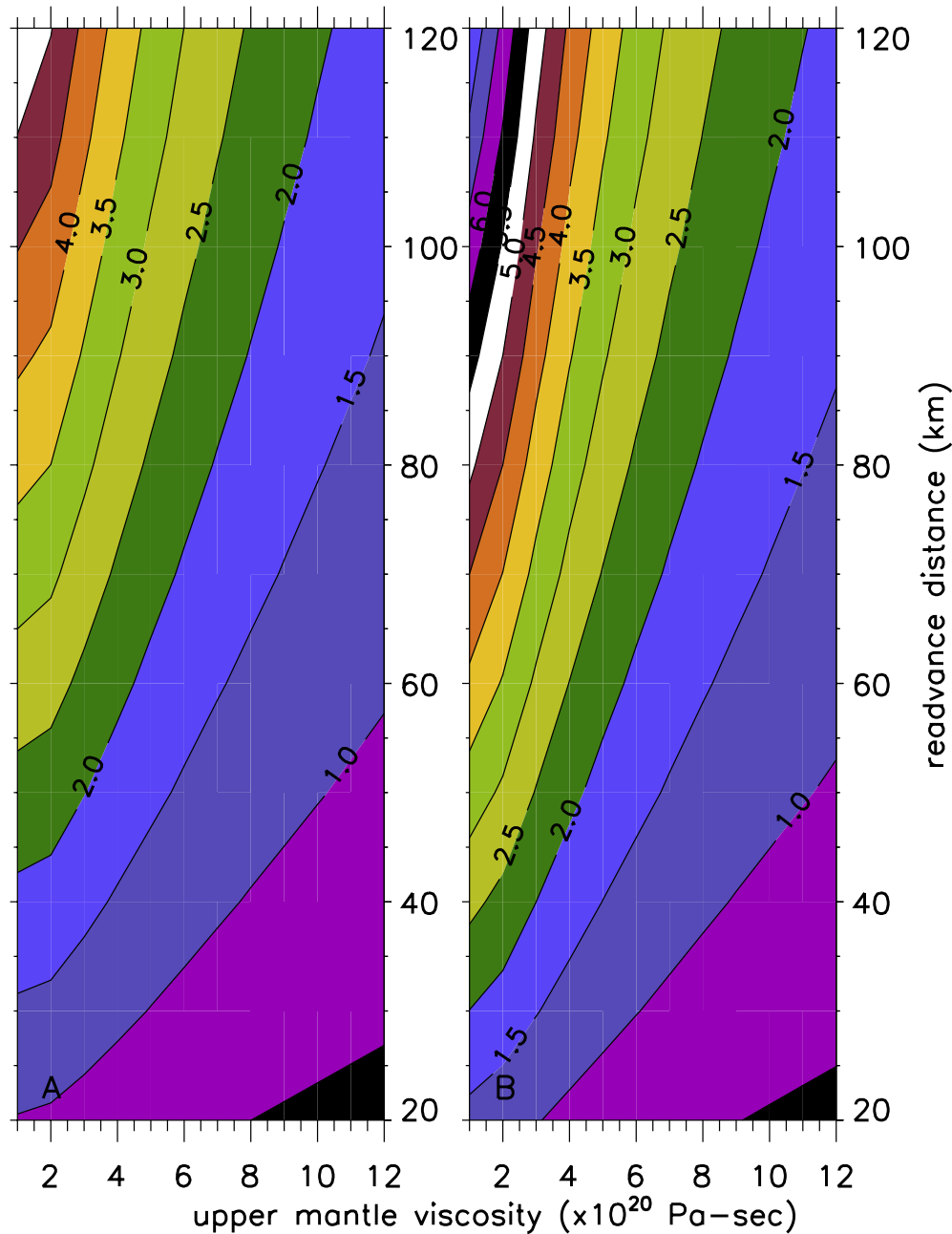


Figure 11. Present-day uplift rates at QAQ1 as a function of upper mantle viscosity and readvance distance. (a) Readvance started 3 ka ago and ended 150 years ago. (b) Readvance started 2 ka ago and ended 150 years ago.

ice core drilling at DYE3, shows that the annual average temperature has decreased by 3°C over the past 4 ka.

[59] *Letréguilly et al.* [1991] employed a climate forcing inferred from the $\delta^{18}\text{O}$ records at DYE 3 to obtain a deglaciation history of the Greenland ice sheet. Their model predicts that the southern portion of the Greenland ice sheet would be only slightly smaller than at present, due to its being situated on a high plateau. The Julianehb Ice Cap, for example, would be only marginally reduced in size at mean annual temperatures of 3°C above present, due to the high elevation of the underlying bedrock plateau. However, there would have been considerable differences between sectors, with a much greater ice sheet retreat occurring in low-lying sectors, such as the Qassimiut lobe.

[60] It is reasonable to assume that the Qassimiut lobe started to readvance about 2–3 ka ago. The increasing load caused by the expansion of the ice sheet would cause local subsidence due to a combination of elastic and viscoelastic effects. A readvance of the Qassimiut lobe is not included in the ICE-5G deglaciation model. Modeling by *Letréguilly et al.* [1991] suggests that the ice sheet margin would have retreated 40–50 km behind the present position for mean annual temperatures of 3°C above present.

[61] We compute the present-day uplift rate at QAQ1 that would be caused by the Earth's viscoelastic response to a readvancing Qassimiut lobe. Results are given in Table 6 for eight different retreat/readvance distances. Each model assumes the readvance started 3 ka ago and ended 150 years

ago, and each uses the VM2 viscosity profile of *Peltier* [2004]. The ice thickness at the margin is 200 m [*Podlech*, 2004] in each model, and increases linearly to 1400 m at a distance of 120 km behind the margin. The entire ice profile is readvanced at a constant rate, so as to cover the specified distance in 2850 years.

[62] The results of uplift rates caused by the readvancing Qassimiut lobe alone are shown in Table 6. These results show that subsidence rates are larger for a larger readvance, a consequence of the fact that there is more cumulative ice added when the margin readvances a greater distance. Those same results after adding the uplift rate predicted by ICE-5G are given and can be compared directly with the GPS observed uplift rate.

[63] The GPS measurements at QAQ1 suggest a secular subsidence rate of -0.3 ± 1.1 mm/a. To explain this subsidence rate, the Table 6 results suggest that a readvance of 10–120 km is needed. However, the model results are sensitive to the choice of viscosity, especially (given the small scale of the Qassimiut lobe and its close proximity to QAQ1) the viscosity in the upper mantle (UM). The Table 6 results all assume the VM2 viscosity profile. VM2 is intended as a global viscosity profile, inferred from observations of rebound worldwide. However, the UM viscosity is largely constrained by relative sea level observations. Also, since most of those observations are in Canada, the VM2 UM viscosity value ($\sim 0.9 \times 10^{21}$ Pa s) is probably most representative of the viscosity within the relatively cold cratonic interior of Canada. It could well be that the UM viscosity beneath southern Greenland is smaller than this. In fact, there are arguments that a smaller value (0.6×10^{21} Pa s) might be more appropriate even under Canada itself [e.g., *Mitrovica*, 1996].

[64] Thus we have also computed QAQ1 uplift rates for many other viscosity profiles, each one using VM2 for the lower mantle, but with a different (constant) value of UM viscosity. Figure 11a shows present-day uplift rates at QAQ1 caused by the Qassimiut lobe alone, as a function of both UM viscosity and readvance distance. Figure 11a assumes that the readvance started 3 ka ago and ended 150 years ago. The 1.3 mm/a contour represents the subsidence rate required to explain the difference between the GPS observation (-0.3 mm/a of subsidence) and the ICE-5G prediction (1.0 mm/a of uplift). For example, to explain this rate with a UM viscosity of 0.1×10^{21} Pa s and a readvance that started 3 ka ago, the readvance distance has to be about 27 km. For a more realistic UM viscosity of $\sim 0.4 \times 10^{21}$ Pa s, a readvance of about 33 km is required. Figure 11b assumes the readvance started 2 ka ago and ended 150 years ago. This gives larger uplift rates, since then all the loading would have been squeezed into a more recent time interval. In this case, readvances of 18 km and 27 km are needed for UM viscosities of 0.1×10^{21} Pa s and 0.4×10^{21} Pa s, respectively.

8. Conclusions

[65] We have analyzed GPS data from 7 GPS sites located at 5 locations along the edge of the Greenland ice sheet. When we correct for the Earth's elastic response to ongoing changes in nearby ice and, the GPS results at KELY transformed to the CE2007 reference frame suggest a secular subsidence rate of -1.2 ± 1.1 mm/a, while the ICE-5G

predicted rate is -3.3 mm/a. The GPS uplift rate of 3.6 ± 1.1 mm/a at THUL is larger than the rate of -0.1 mm/a predicted by ICE-5G. The GPS measurements at SCBB suggest a secular uplift rate of 0.0 ± 1.1 mm/a, while ICE-5G predicts 2.0 mm/a. Also, the GPS measurements at KULU suggest a secular subsidence rate of -0.4 ± 1.1 mm/a, while ICE-5G predicts -1.7 mm/yr. Tide gauge results at Nuuk show a secular subsidence rate of -2.2 ± 1.3 mm/a. The subsidence rate is somewhat larger than the rate of -1.0 mm/a obtained by *Dietrich et al.* [2005] using differential GPS. The ICE-5G deglaciation model of *Peltier* [2004] predicts a significantly larger secular subsidence rate, of -3.3 mm/a.

[66] In each of these cases, the difference between the observed and predicted rates is on the order of 1.3–3.7 mm/a, though the sign of that difference is not always the same. A explanation is that ICE-5G does not exactly reproduce the correct rebound signal. For example, the ICE-5G predicted present-day uplift in northwest Greenland is dominated by the presence of a dome over Ellesmere Island, where the predicted maximum present-day uplift rate is about 8 mm/a. The deviation between observed and predicted uplift of about 3.7 mm/a at THUL can be explained by expanding the dome further to the east or by increasing its thickness during LGM.

[67] The ICE-5G subsidence at KELY and NUUK is caused by a readvance of the ice margin in west Greenland (between latitude of 62°N and 72°N) to its current location during the last 8000 years. The GPS and tide gauge observations thus suggest that the ICE-5G readvance of the margin in this region could be too large.

[68] GPS results at QAQ1 suggest (after removing the Earth's elastic response to ongoing changes in ice) a secular subsidence rate of -0.3 ± 1.1 mm/a, while the ICE-5G model predicts an uplift rate of 1.0 mm/a. The ICE-5G model assumes the ice sheet margin in west Greenland (between latitudes 62°N and 72°N) readvanced during the last 8000 years to its current position. The modeled readvance is a maximum of 40–60 km near Kangerlussuaq, decreasing to just a few km at 62°N and 72°N . ICE-5G assumes no ice sheet readvance in southwest or south Greenland, including no readvance of the Qassimiut lobe. *Létréguilly et al.* [1991] showed, however, that the margin of the Qassimiut lobe was probably about 40 km or more further inland from its present position a few thousand years ago. The difference of 1.3 ± 1.1 mm/a between the ICE-5G predicted uplift rate and our observed uplift rate at QAQ1 can tentatively be explained by readvancing the Qassimiut lobe over a distance of about 33 km during the last ~ 3 ka and using a UM viscosity of 0.4×10^{21} Pa s.

[69] **Acknowledgments.** We acknowledge useful suggestions provided by an anonymous reviewer, an Associate Editor, Jeffrey Freymueller, and Kevin Fleming that improved the content of this article. We thank Palle Bo Nielsen for access to the Nuuk tide gauge data; Finn Bo Madsen and Ole B Hansen for access to the GPS data at Thule, Scoresbysund, and Qaqortoq; we thank Anker Weidick for discussions regarding the readvance of the Qassimiut lobe. We thank Geoffrey Blewitt for providing us with his estimate of the drift between the ITRF2000 and preliminary ITRF2005P reference frames. We thank Michael Heflin for providing us with his transformation parameters (x files) from the free network estimates to the ITRF2005 reference frame. We thank Per Knudsen for comments on the manuscript. John Wahr's effort was partially supported by NASA grants NNG04GF02G and NNX06AH37G to the University of Colorado.

References

- Altamimi, Z., P. Sillard, and C. Boucher (2002), ITRF2000: A new release of the International Terrestrial Reference Frame for earth science applications, *J. Geophys. Res.*, **107**(B10), 2214, doi:10.1029/2001JB000561.
- Altamimi, Z., X. Collilieux, J. Legrand, B. Garayt, and C. Boucher (2007), ITRF2005: A new release of the International Terrestrial Reference Frame based on time series of station positions and Earth Orientation Parameters, *J. Geophys. Res.*, **112**, B09401, doi:10.1029/2007JB004949.
- Argus, D. (2007), Defining the translational velocity of the reference frame of Earth, *Geophys. J. Int.*, **169**, 830–838, doi:10.1111/j.1365-246X.2007.03344.x.
- Boehm, J., B. Werl, and H. Schuh (2006), Troposphere mapping functions for GPS and very long baseline interferometry from European Centre for Medium-Range Weather Forecasts operational analysis data, *J. Geophys. Res.*, **111**, B02406, doi:10.1029/2005JB003629.
- Chambers, D. P., J. C. Ries, C. K. Shum, and B. D. Tapley (1998), On the use of tide gauges to determine altimeter drift, *J. Geophys. Res.*, **103**(C6), 12,885–12,890.
- Chambers, D. P., J. C. Ries, and T. J. Urban (2003), Calibration and verification of Jason-1 using global along-track residuals with TOPEX, *Mar. Geod.*, **26**(3), 305–317.
- Dahl-Jensen, D., K. Mosegaard, N. Gundestrup, G. D. Clow, S. J. Johnsen, A. W. Hansen, and N. Balling (1998), Past temperatures directly from the Greenland ice sheet, *Science*, **282**(5387), 268–271.
- Dietrich, R., A. Rulke, and M. Scheinert (2005), Present-day vertical crustal deformations in West Greenland from repeated GPS observations, *Geophys. J. Int.*, **163**(3), 865–874.
- Dietrich, R., H.-G. Maas, M. Baessler, A. Rulke, A. Richter, E. Schwalbe, and P. Westfeld (2007), Jakobshavn Isbr, West Greenland: Flow velocities and tidal interaction of the front area from 2004 field observations, *J. Geophys. Res.*, **112**, F03S21, doi:10.1029/2006JF000601.
- Farrell, W. (1972), Deformation of the Earth by surface loads, *Rev. Geophys.*, **10**, 761–797.
- Fleming, K., and K. Lambeck (2004), Constraints on the Greenland Ice Sheet since the Last Glacial Maximum from sea-level observations and glacial-rebound models, *Quat. Sci. Rev.*, **23**, 1053–1077.
- Fredskild, B. (1973), Studies in vegetational history of Greenland, *Medd. Groenland*, **198**, 245 pp.
- Fu, L.-L., and A. Cazenave (2000), *Satellite Altimetry and Earth Sciences: A Handbook of Techniques and Applications*, Academic, 463 pp., San Diego, Calif.
- Howat, I. M., I. Joughin, S. Tulaczyk, and S. Gogineni (2005), Rapid retreat and acceleration of Helheim Glacier, east Greenland, *Geophys. Res. Lett.*, **32**, L22502, doi:10.1029/2005GL024737.
- Huybrechts, P. (1992), The antarctic ice sheet and environmental change: A three-dimensional study, *Rep. Pol. Res.* **99**, Alfred Wegener Inst., Bremerhaven, Germany.
- Huybrechts, P. (1996), Basal temperature conditions of the Greenland ice sheet during the glacial cycles, *Ann. Glaciol.*, **23**, 226–236.
- Johansson, J. M., et al. (2002), Continuous GPS measurements of postglacial adjustment in Fennoscandia: 1. Geodetic results, *J. Geophys. Res.*, **107**(B8), 2157, doi:10.1029/2001JB000400.
- Joughin, I., W. Abdalati, and M. Fahnestock (2004), Large fluctuations in speed on Greenland's Jakobshavn Isbr glacier, *Nature*, **432**, 608–610, doi:10.1038/nature03130.
- Khan, S. A., J. Wahr, L. A. Stearns, G. S. Hamilton, T. van Dam, K. M. Larson, and O. Francis (2007), Elastic uplift in southeast Greenland due to rapid ice mass loss, *Geophys. Res. Lett.*, **34**, L21701, doi:10.1029/2007GL031468.
- Krabill, W., et al. (2004), Greenland Ice Sheet: Increased coastal thinning, *Geophys. Res. Lett.*, **31**, L24402, doi:10.1029/2004GL021533.
- Landvik, J. Y., A. Weidick, and A. Hansen (2001), The glacial history of the Hans Tausen Iskappe and the last glaciation of Peary Land, North Greenland, *Medd. Groenland Geosci.*, **39**, 27–44.
- Létréguilly, A., P. Huybrechts, and N. Reeh (1991), Steady-state characteristics of the Greenland ice sheet under different climates, *J. Glaciol.*, **37**, 149–157.
- Leuliette, E. W., R. S. Nerem, and G. T. Mitchum (2004), Calibration of TOPEX/Poseidon and Jason altimeter data to construct a continuous record of mean sea level change, *Mar. Geod.*, **12**, 79–94.
- Mitchum, G. T. (1994), Comparison of TOPEX sea surface heights and tide gauge sea levels, *J. Geophys. Res.*, **99**, 24,541–24,554.
- Mitchum, G. T. (1998), Monitoring the stability of satellite altimeters with tide gauges, *J. Atmos. Oceanic Technol.*, **15**(3), 721–730.
- Mitchum, G. T. (2000), An improved calibration of satellite altimetric heights using tide gauge sea levels with adjustment for land motion, *Mar. Geod.*, **23**(3), 145–166.
- Mitrovica, J. X. (1996), Haskell [1935] revisited, *J. Geophys. Res.*, **101**(B1), 555–569.
- Mitrovica, J. X., J. Wahr, I. Matsuyama, and A. Paulson (2005), The rotational stability of an Ice Age Earth, *Geophys. J. Int.*, **161**, 491–506.
- Niell, A. E. (1996), Global mapping functions for the atmosphere delay at radio wavelengths, *J. Geophys. Res.*, **101**(B2), 3227–3246.
- Peltier, W. R. (1994), Ice Age paleotopography, *Science*, **265**, 195–201.
- Peltier, W. R. (2004), Global glacial isostasy and the surface of the Ice-Age Earth: the ICE-5G (VM2) model and GRACE, *Annu. Rev. Earth Planet. Sci.*, **32**, 111–149, doi:10.1146/annurev.earth.32.082503.144359.
- Podlech, S. (2004), The Qassimiut Ice Lobe, South Greenland, Ph.D thesis, Natl. Geol. Unders. Danmark Groenland, Fac. of Sci., Univ. of Copenhagen, Copenhagen, Denmark.
- Press, W. H., W. T. Vetterling, S. A. Teukolsky, and B. P. Flannery (1992), *Numerical Recipes in FORTRAN 77*, 2nd ed., pp. 494–502, Cambridge Univ. Press, New York.
- Ray, R. (1999), A Global ocean tide model from T/P altimetry: GOT99.2, *NASA Tech. Memo.*, TM-209478.
- Rignot, E., and P. Kanagaratnam (2006), Changes in the velocity structure of the Greenland ice sheet, *Science*, **311**, 986–990, doi:10.1126/science.1121381.
- Stearns, L. A., and G. S. Hamilton (2007), Rapid volume loss from East Greenland outlet glaciers quantified using repeat stereo satellite imagery, *Geophys. Res. Lett.*, **34**, L05503, doi:10.1029/2006GL028982.
- Tarasov, L., and W. R. Peltier (2002), Greenland glacial history and local geodynamic consequences, *Geophys. J. Int.*, **150**, 198–229.
- Tregoning, P., and T. A. Herring (2006), Impact of a priori zenith hydrostatic delay errors on GPS estimates of station heights and zenith total delays, *Geophys. Res. Lett.*, **33**, L23303, doi:10.1029/2006GL027706.
- van Tatenhove, F., J. van der Meer, and E. Koster (1996), Implications for deglaciation chronology from new AMS age determinations in central West Greenland, *Quat. Res.*, **45**, 245–253.
- Vey, S., R. Dietrich, M. Fritsche, A. Rulke, M. Rothacherl, and P. Steigenberger (2006), Influence of mapping function parameters on global GPS network analyses: Comparisons between NMF and IMF, *Geophys. Res. Lett.*, **33**, L01814, doi:10.1029/2005GL024361.
- Wahr, J., T. van Dam, K. M. Larson, and O. Francis (2001), Geodetic measurements in Greenland and their implications, *J. Geophys. Res.*, **106**(B8), 16,567–16,582.
- Wdowski, S., Y. Bock, J. Zhang, P. Fang, and J. Genrich (1997), Southern California Permanent GPS Geodetic Array: Spatial filtering of daily positions for estimating coseismic and postseismic displacements induced by the 1992 Landers earthquake, *J. Geophys. Res.*, **102**(B8), 18,057–18,070.
- Weidick, A., M. Kelly, and O. Bennike (2004), Late Quaternary development of the southern sector of the Greenland Ice Sheet, with particular reference to the Qassimiut lobe, *BOREAS*, **33**(4), 285–299.
- Zlotnicki, V., and P. Callahan (2002), TOPEX and Jason Microwave Radiometer assessment against DMSP-SSM/I and TRMM/TMI, paper presented at Jason-1/TOPEX/Poseidon Science Working Team Meeting, Biarritz, France.
- Zumberge, J. F., M. B. Heflin, D. C. Jefferson, M. M. Watkins, and F. H. Webb (1997), Precise point positioning for the efficient and robust analysis of GPS data from large networks, *J. Geophys. Res.*, **102**(B3), 5005–5017.

O. Francis and T. van Dam, Faculty of Sciences, Technology and Communication, University of Luxembourg, 162 A, Avenue de la Faïencerie, L-1511 Luxembourg, Luxembourg.

S. A. Khan, Department of Geodesy, Danish National Space Center, Technical University of Denmark, Juliane Maries Vej 30, Copenhagen Ø, Denmark. (abbas@space.dtu.dk)

K. M. Larson, Department of Aerospace Engineering Sciences, UCB 429, University of Colorado, Boulder, CO 80309-0429, USA.

E. Leuliette, Colorado Center for Astrodynamics Research, University of Colorado, Campus Box 431, Boulder, CO 80309-0431, USA.

J. Wahr, Department of Physics, University of Colorado, Campus Box 390, Boulder, CO 80309-0390, USA.